Supporting Information for:

Molecular-Level Insights into the Seasonal Formation of Organosulfates in a Mountain Atmosphere

Ting Wang[1], Youwei Hong[*,2], Jing Duan[3], Liyuan Zhou[1], Ying Wang[2], Wei Xu[*,1]

[1]State Key Laboratory of Advanced Environmental Technology, Institute of Urban Environment, Chinese Academy of Sciences, Xiamen, 361021, China

[2]Quanzhou Normal University, College of Resources and Environmental Sciences, Quanzhou, 362000, China

[3]State Key Laboratory of Loess Science, Institute of Earth Environment, Chinese Academy of Sciences, Xi'an 710061, China

Correspondence to: Wei Xu (wxu@iue.ac.cn), Youwei Hong (ywhong25062@qztc.edu.cn)

Table of Contents: Supporting Figures and Tables

Figure S1. Percentage of number and abundance of potential OSs to CHOS and NOSs to CHONS formulas in summer and winter. 5

Figure S2. Carbon oxidation state (OS_c) as a function of carbon number for OSs and nitrooxy-OSs in summer and winter. Each point represents an individual molecular formula, and marker size reflects its relative signal intensity....................5

Figure S3. Time series of meteorological parameters (T and RH), gaseous pollutants (O_3, SO_2, NO_2, and CO), and chemical composition of $PM_{2.5}$ (OM, NO_3^-, SO_4^{2-}, NH_4^+, Cl^-) during the sampling periods in summer and winter. 6

Figure S4. Relationship between C_2/C_3 OS abundance and total OS abundance (a), and box plot of C_2/C_3 OS to OSi ratios in summer and winter..................................6

Figure S5. Distribution in signal abundance (top) and percentage (bottom) of different OS classes in summer and winter. 7

Figure S6. Seasonal variation of O_x, T, pH, SO_4^{2-}, NH_4^+, NO_3^-, ALWC, and RH....7

Figure S7. Correlations between OSs with meteorological conditions, gaseous pollutants, and chemical components in summer and winter. 8

Figure S8. ALWC-to-dry $PM_{2.5}$ mass ratios in summer and winter..........................8

Table S1. Organosulfates identified in this study, including formula, mass, retention time (RT), proposed structure, common name, and references. ……………….…10

Text S1. Chemical Analysis.

The extracts were analyzed using a Dionex Ultimate 3000 UHPLC (Thermo Fisher Scientific, Waltham, US) coupled to an Orbitrap Exploris 120 mass spectrometer (Thermo Fisher Scientific, Waltham, US). A HSS T3 column (2.1 × 100 mm, 1.8 μm particle size) was used to separate the organics in the sample extracts. A binary gradient elution was applied at a flow rate of 0.3 mL min^{-1}, with mobile phase A of 0.1% acetic acid in water and mobile phase B of 0.1% acetic acid in methanol. The gradient elution was set as follows: mobile phase B was held at 1% at the beginning (held on 2.7 min), and linearly increased to 54% after 15.2 min (held on 1.0 min), followed by linear increase to 90% after 7.5 min (held on 0.2 min), and finally decrease to 1% after 1.8 min (held on 9.3 min).

Text S2. ALWC and aerosol pH

The aerosol liquid water content (ALWC) and aerosol pH were estimated using the thermodynamic model ISORROPIA-II, constrained by measured inorganic aerosol composition (NH_4^+, SO_4^{2-}, NO_3^-, and Cl^-), ambient temperature, and RH as input parameters. The model was operated in metastable mode, assuming fully deliquescent particles without solid phases, to simulate the thermodynamic equilibrium and phase state of inorganic species and derive ALWC.

The aerosol liquid water content (ALWC) and aerosol pH were estimated using the thermodynamic model ISORROPIA-II, constrained by measured inorganic aerosol composition (NH_4^+, SO_4^{2-}, NO_3^-, and Cl^-), ambient temperature, and RH. The model was operated in metastable mode, assuming fully deliquescent particles without solid phases. ALWC was obtained from model as the predicted particle-phase liquid water associated with inorganic species.

Aerosol pH was calculated as:

$$pH = -\log10([H^+]\_aq)$$

where $[H^+]\_aq$ represents the molality of hydronium ions in the particle liquid water predicted by model.

Text S3. Calculation of SOR and NOR

The sulfur oxidation rate (SOR) and nitrogen oxidation rate (NOR) were calculated to evaluate the secondary processes. The calculations are as follows:

$$SOR = SO_4^{2-}(p)/[SO_2(g) + SO_4^{2-}(p)]$$

$$NOR = NO_3^{-}(p)/[NO_2(g) + NO_3^{-}(p)]$$

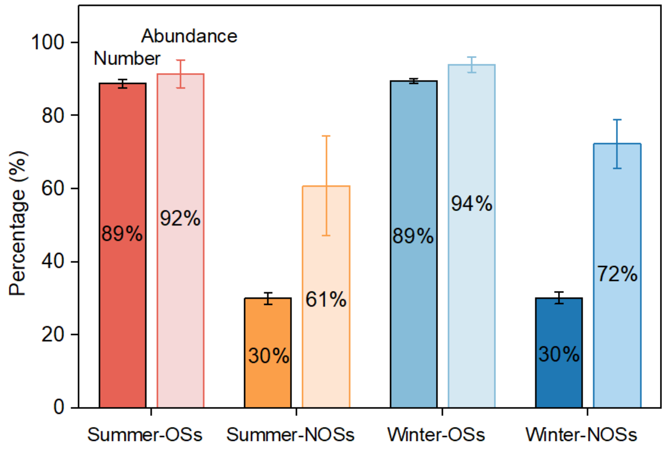

Figure S1. Percentage of number and abundance of potential OSs to CHOS and NOSs to CHONS formulas in summer and winter.

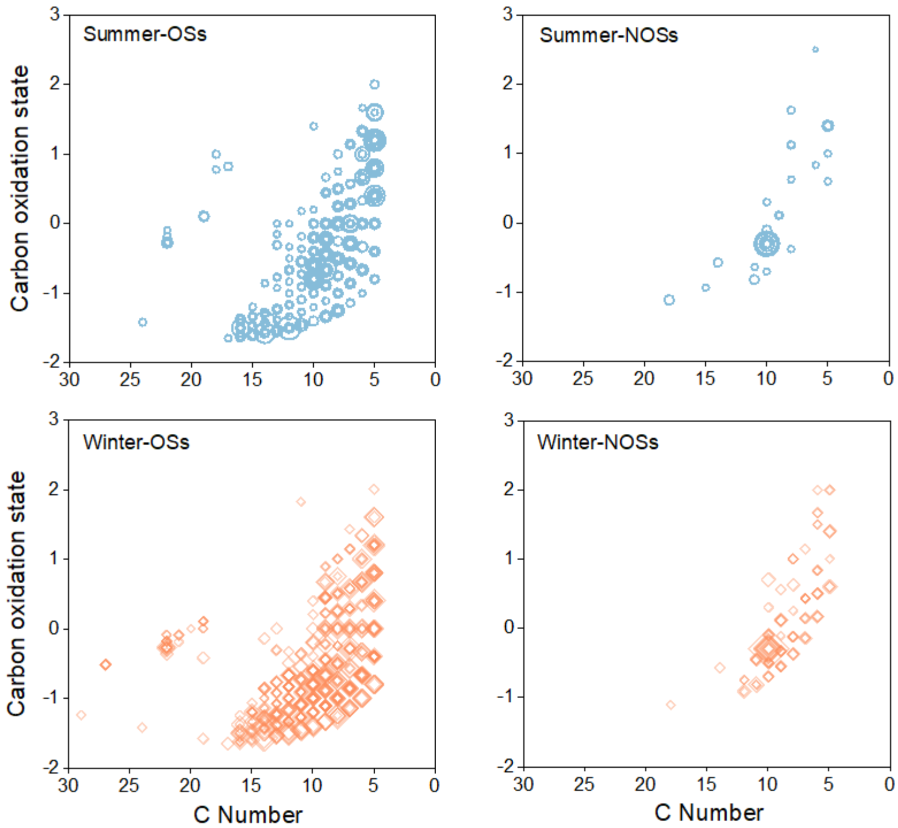

Figure S2. Carbon oxidation state ($\overline{OS}_c$) as a function of carbon number for OSs and nitrooxy-OSs in summer and winter. Each point represents an individual molecular formula, and marker size reflects its relative signal intensity.

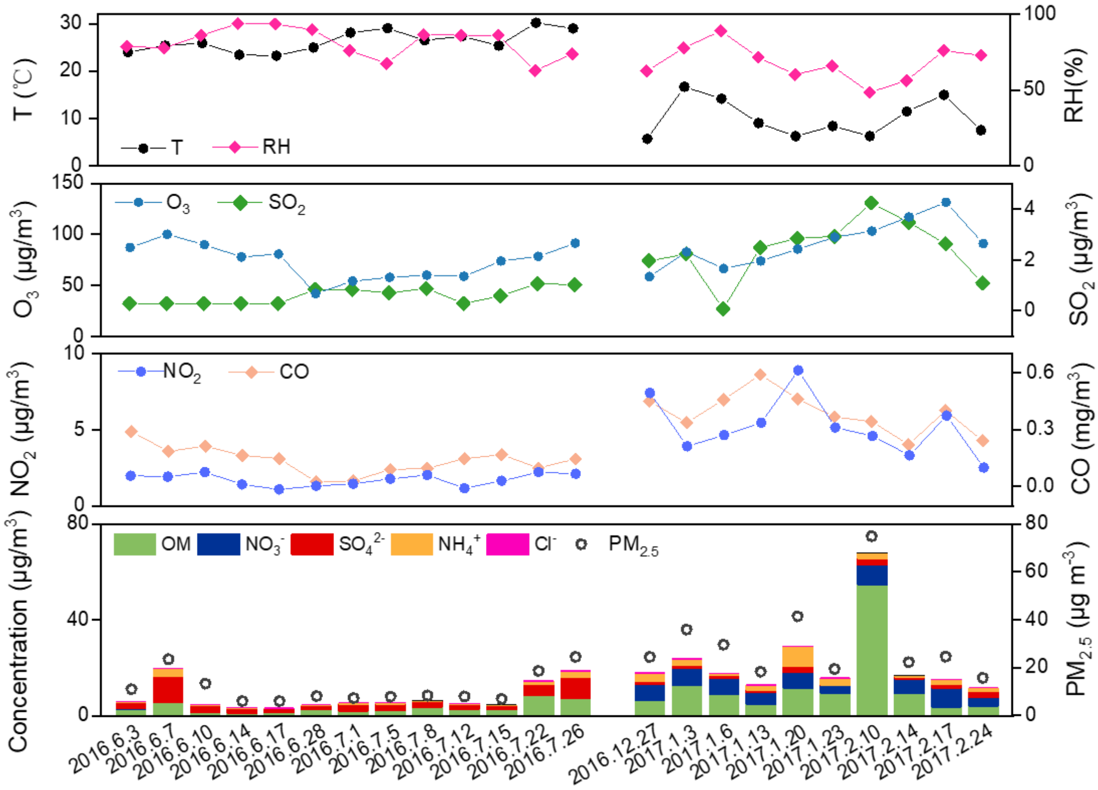

Figure S3. Time series of meteorological parameters (T and RH), gaseous pollutants (O_3, SO_2, NO_2, and CO), and chemical composition of $PM_{2.5}$ (OM, NO_3^-, SO_4^{2-}, NH_4^+, Cl^-) during the sampling periods in summer and winter.

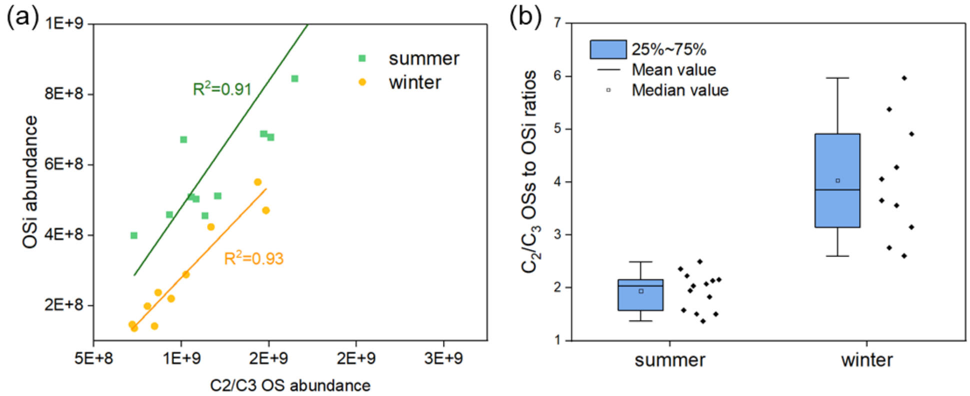

Figure S4. Relationship between C_2/C_3 OS abundance and total OS abundance (a), and box plot of C_2/C_3 OS to OSi ratios in summer and winter.

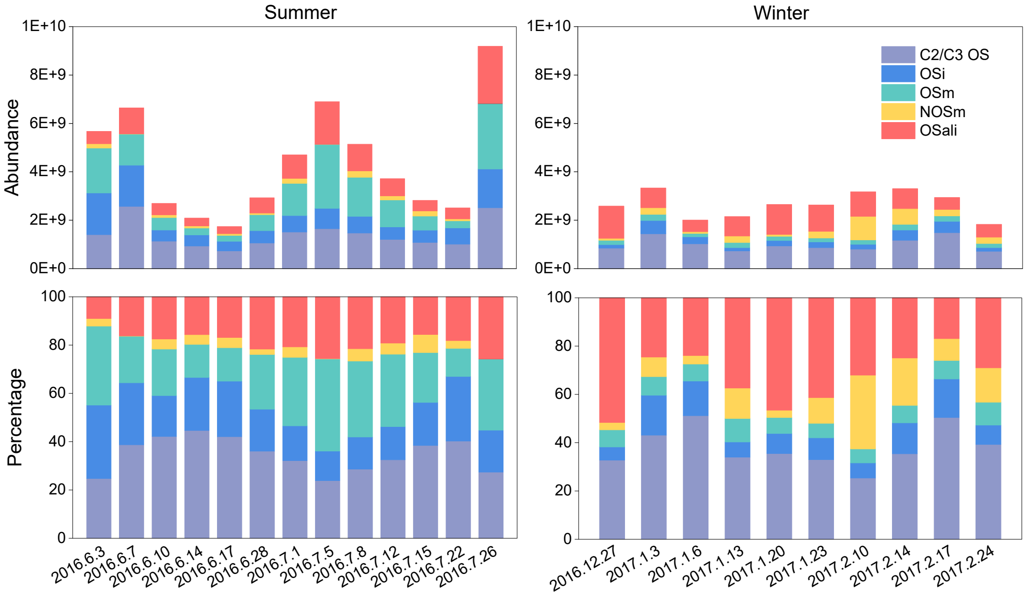

Figure S5. Distribution in signal abundance (top) and percentage (bottom) of different OS classes in summer and winter.

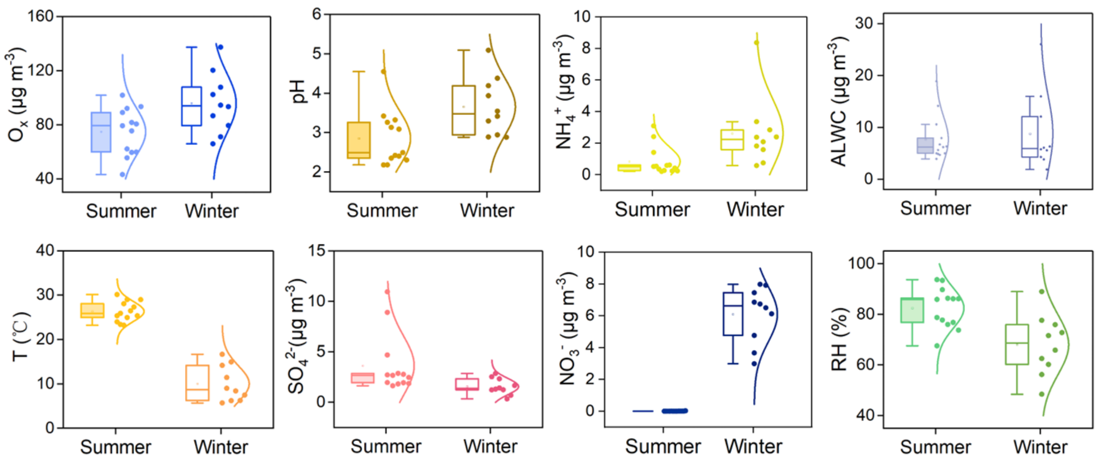

Figure S6. Seasonal variation of O_x, T, pH, SO_4^{2-}, NH_4^+, NO_3^-, ALWC, and RH.

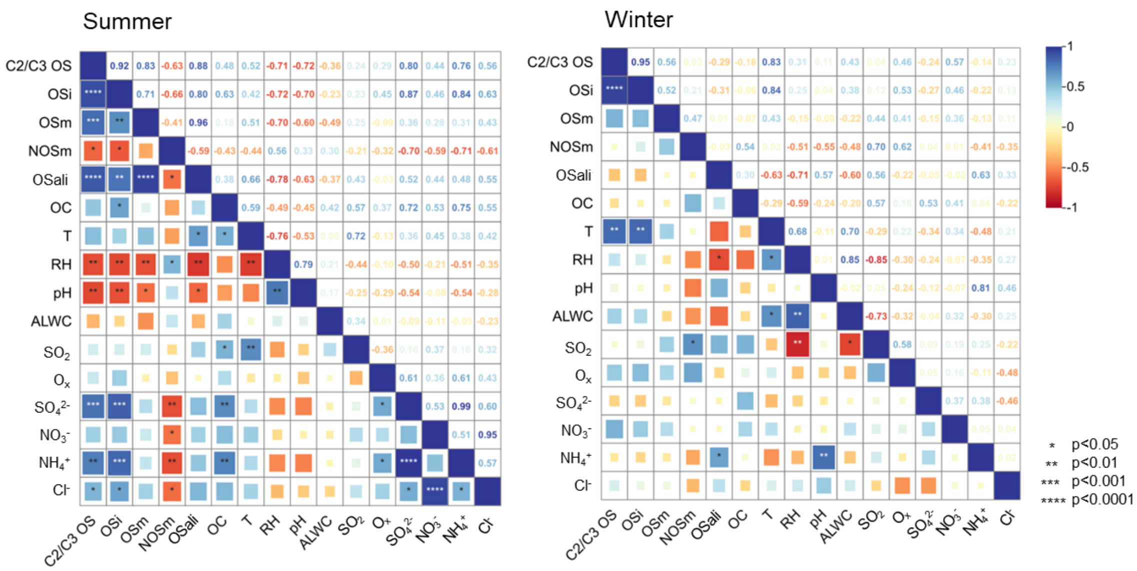

Figure S7. Correlations between OSs with meteorological conditions, gaseous pollutants, and chemical components in summer and winter.

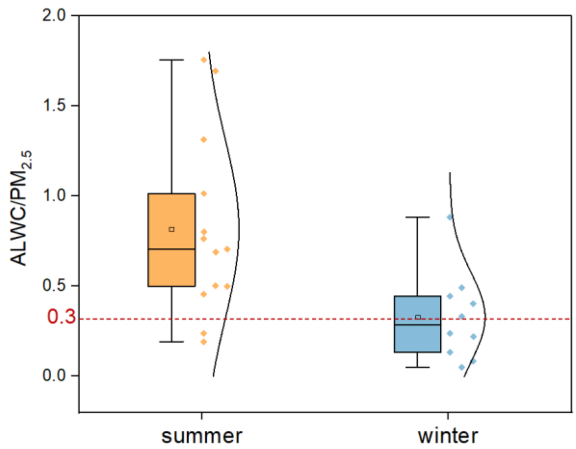

Figure S8. ALWC-to-dry $PM_{2.5}$ mass ratios in summer and winter.

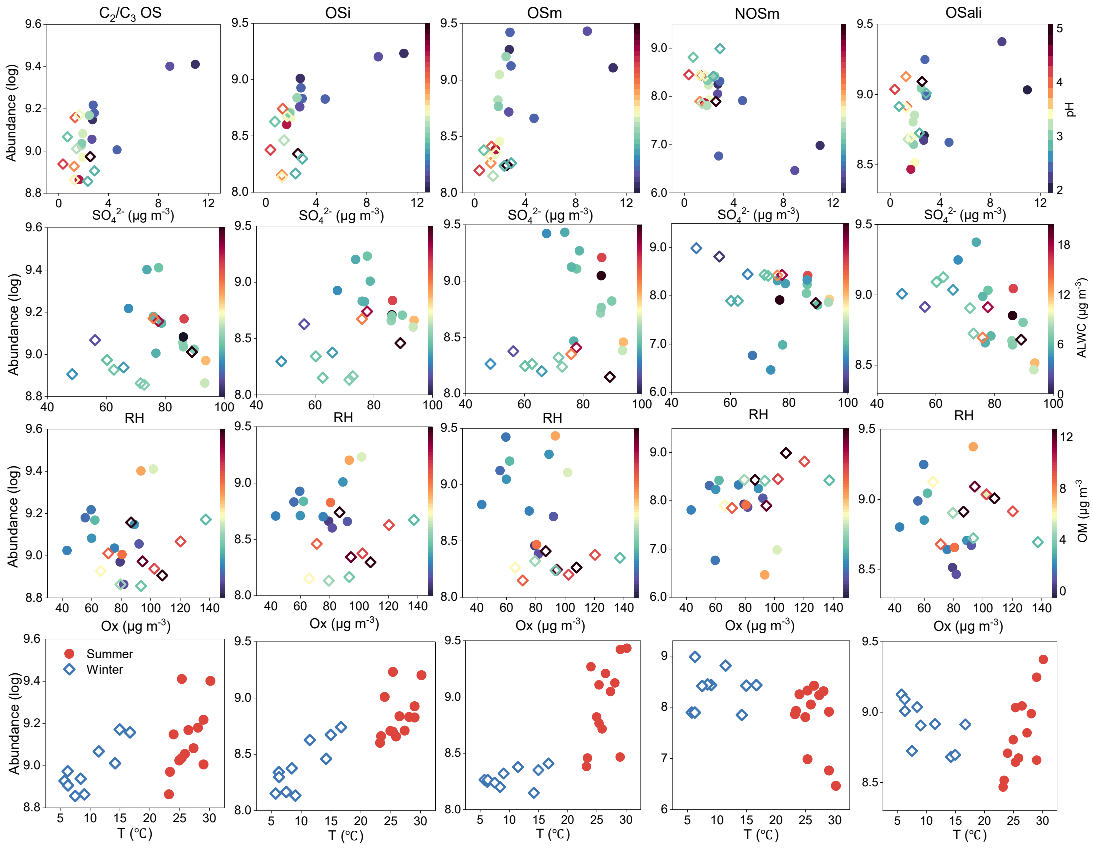

Figure S9. Scatter plots showing the relationships between OS abundances and atmospheric variables for summer and winter samples.

Table S1. Organosulfates identified in this study, including formula, mass, retention time (RT), proposed structure, common name, and references.

	Classes	[M-H]⁻ Formula	[M-H]⁻ Mass	RT (min)	Error (ppm)	Proposed structure	Common name	References
1	C2/C3 OSs	C2H3O5S⁻	138.9704	1.1	-2.139	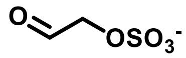		(Yang et al. 2025)
2	C2/C3 OSs	C3H7O4S⁻	139.0068	3.26, 3.71	-1.458	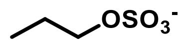		
3	C2/C3 OSs	C3H5O5S⁻	152.9860	1.19, 1.6	0.8	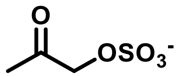	Hydroxyacetone Sulfate (HAS)	(Hughes et al. 2019) (Cai et al. 2020)
4	C2/C3 OSs	C2H3O6S⁻	154.9651	1.14, 1.33	1.72	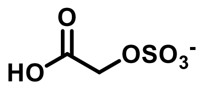	Glycolic acid Sulfate (GAS)	(Hughes et al., 2019) (Cai et al., 2022)
5	C2/C3 OSs	C3H5O6S⁻	168.9808	1.2, 1.72	-2.26	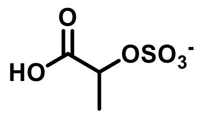	Lactic acid Sulfate (LAS)	(Hughes et al., 2019) (Cai et al., 2022)
6	Isoprene OSs	C4H7O5S⁻	167.0016	3.25	-2.08	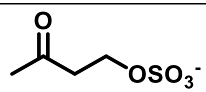		(Yang et al., 2025)
7	Isoprene OSs	C5H9O6S⁻	197.0120	2.32, 4.52	-2.294	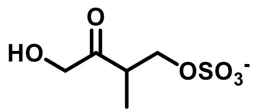		(Hughes et al., 2019)
8	Isoprene OSs	C4H7O7S⁻	198.9913	1.18, 1.49	-2.646	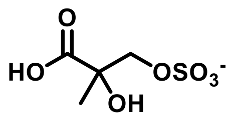		(Hughes et al., 2019) (Cai et al., 2022)

9	Isoprene OSs	C5H7O7S⁻	210.9913	1.19, 2.19	-2.258	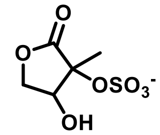		(Hughes et al., 2019) (Cai et al., 2022)
10	Isoprene OSs	C5H9O7S⁻	213.0069	1.17, 1.38, 1.86	-2.519	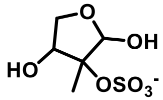		(Hughes et al., 2019) (Cai et al., 2022)
)11	Monoterpene OSs	C10H15O4S⁻	231.0692	23.27	-1.917	Unknown		(Cai et al., 2022)
12	Monoterpene OSs	C9H15O5S⁻	235.0642	12.22	-1.393	Unknown		
13	Monoterpene OSs	C7H11O7S⁻	239.0225	6.33, 7.92	-2.329	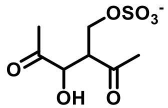		(Hughes et al., 2019)
14	Monoterpene OSs	C10H15O5S⁻	247.1642	14.83	-1.326	Unknown		(Yang et al., 2025)
15	Monoterpene OSs	C10H17O5S⁻	249.0799	16.93	-1.436	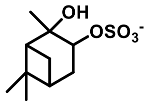	α-pinene OSs	(Cai et al., 2022)
16	Monoterpene OSs	C10H17O5S⁻	249.0799	17.59	-1.355	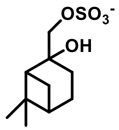	β-pinene OSs	(Cai et al., 2022)
17	Monoterpene OSs	C10H17O5S⁻	249.0791	16.58, 17.98	-4.607	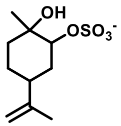	Limonene OSs	(Cai et al., 2022)
18	Monoterpene OSs	C9H17O6S⁻	253.0747	17.24	-1.866	Unknown		

19	Monoterpene OSs	C10H17O7S⁻	281.0694	12.27,12.66,13.11	-2.301	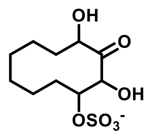		(Hughes et al., 2019)
20	Monoterpene NOSs	C10H16NO7S⁻	294.0646	20.14, 22.52, 22.66	-1.312	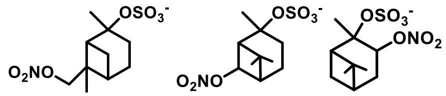		(Cai et al., 2022)
21	Aliphatic-like OSs	C4H9O4S⁻	153.0224	6.98, 7.58	-1.979	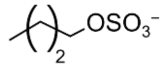		
22	Aliphatic-like OSs	C6H13O4S⁻	181.0537	17.28, 17.84	-1.507	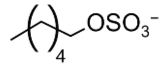		
23	Aliphatic-like OSs	C7H15O4S⁻	195.0693	19.82, 20.21, 21.16	-1.143	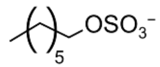		(Yang et al., 2025)
24	Aliphatic-like OSs	C8H17O4S⁻	209.0850	22.96, 23.32, 23.93	-1.258	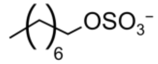		(Yang et al., 2025)
25	Aliphatic-like OSs	C9H19O4S⁻	223.1006	24.96	-1.493	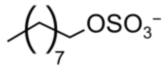		(Yang et al., 2025)
26	Aliphatic-like OSs	C10H21O4S⁻	237.1163	26.96, 27.06	-0.941	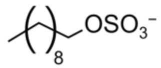		(Yang et al., 2025)
27	Aliphatic-like OSs	C12H25O4S⁻	265.1475	26.67	-1.559	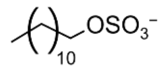		
28	Aliphatic-like OSs	C4H7O4S⁻	151.0067	13.37	-2.071	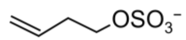	Butenyl sulfate	
29	Aliphatic-like OSs	C6H11O4S⁻	179.0381	12.31, 12.49, 12.56	-0.909	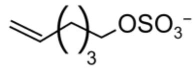	Hexenyl sulfate	
30	Aliphatic-like OSs	C7H13O4S⁻	193.0538	16.82	-0.896	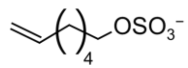	Heptenyl sulfate	

31	Aliphatic-like OSs	C8H15O4S⁻	207.0695	20.06	-1.222	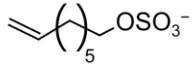	Octenyl sulfate
32	Monoterpene OSs	C9H17O4S⁻	221.0852	22.32	-0.647	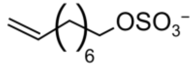	Nonyl sulfate
33	Aliphatic-like OSs	C4H9O5S⁻	169.0173	2.33, 2.59, 2.79	-1.7	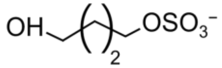	Hydroxybutyl sulfate
34	Aliphatic-like OSs	C5H11O5S⁻	183.0331	4.16	-0.751	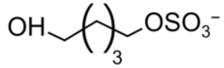	Hydroxypentyl sulfate
35	Aliphatic-like OSs	C8H17O5S⁻	225.0799	19.01	-1.367	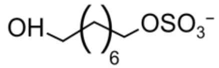	Hydroxyoctyl sulfate

References:

Yang, T., Xu, Y., Wang, Y.-C., Ma, Y.-J., Xiao, H.-W., Xiao, H. and Xiao, H.-Y.: Non-biogenic sources are an important but overlooked contributor to aerosol isoprene-derived organosulfates during winter in northern China. Atmospheric Chemistry and Physics, 25, 2967-2978, 2025.

Hughes, D. D. and Stone, E. A.: Organosulfates in the Midwestern United States: abundance, composition and stability. Environmental Chemistry, 16, 312-322, 2019.

Cai, D., Wang, X., Chen, J. and Li, X.: Molecular Characterization of Organosulfates in Highly Polluted Atmosphere Using Ultra-High-Resolution Mass Spectrometry. Journal of Geophysical Research: Atmospheres, 125, 2020.